ACTA MECHANICA SINICA, Vol.20, No.2, April 2004 ISSN 0567-7718
The Chinese Society of Theoretical and Applied Mechanics
Chinese Journal of Mechanics Press, Beijing, China
Allerton Press, INC., New York, U.S.A.

NUMERICAL ANALYSIS OF THEORETICAL MODEL OF THE RF MEMS SWITCHES*

ZHANG Lixian (张立宪)[1] YU Tongxi (余同希)[2] ZHAO Yapu (赵亚溥)[1,†]

[1](*State Key Laboratory of Nonlinear Mechanics (LNM), Institute of Mechanics, Chinese Academy of Sciences, Beijing* 100080, *China*)

[2](*Department of Mechanical Engineering, Hong Kong University of Science and Technology, Clear Water Bay, Kowloon, Hong Kong SAR, China*)

ABSTRACT: An improved electromechanical model of the RF MEMS (radio frequency microelectromechanical systems) switches is introduced, in which the effects of intrinsic residual stress from fabrication processes, axial stress due to stretching of beam, and fringing field are taken into account. Four dimensionless numbers are derived from the governing equation of the developed model. A semi-analytical method is developed to calculate the behavior of the RF MEMS switches. Subsequently the influence of the material and geometry parameters on the behavior of the structure is analyzed and compared, and the corresponding analysis with the dimensionless numbers is conducted too. The quantitative relationship between the presented parameters and the critical pull-in voltage is obtained, and the relative importance of those parameters is given.

KEY WORDS: RF MEMS, axial stretching, residual stress, fringing field, critical pull-in voltage

1 INTRODUCTION

In recent years, the MEMS (microelectromechanical systems) technology has grown rapidly all over the world. The RF (radio frequency) MEMS is relatively new one which has already generated a tremendous amount of excitement because of the enhanced performances and reduced cost[1]. As novel device, the RF MEMS switches have a myriad application future in wireless communication and radar system[2~4]. Compared with conventional switches widely used in microwave and monolithic microwave integrated circuits (MMICs) such as p-i-n (PIN) diodes and field-effect transistor (FET) switches, the RF MEMS switches offer high isolation, high frequency, good Q-factor, low return loss, low insertion loss and power consumption.

Since the membrane-based switch on silicon reported by Petersen[5] as early as 1979, lots of researches based on various structures, fabrication processes, and activated principles have been reported[1]. The switch we study is electrostatically actuated and is doubly supported. A doubly supported RF MEMS switch usually consists of two parallel plates. One plate is fixed on the substrate and the other is formed by Au or Cu thin film prepared by electroplating process. A schematic of a doubly supported RF MEMS switch is shown in Fig.1. While a bias voltage is applied between the fixed and movable plates of switch, the movable plate could move down onto the fixed substrate subjected to electrostatic force. The device controls mechanical electric current or signal by using the on/off impedance radio. When the threshold (pull-in) voltage is reached, the switch is in the down state or blocking state, and when no voltage is applied it is in the up state or pass-through state.

An accurate theoretical model may efficiently lead the design and computation, and reduce the re-

Received 6 August 2003
*The project supported by the National Natural Science Foundation of China, the Chinese Academy of Sciences, the RGC/NSFC Joint Research Scheme (N-HKUST 601/01) and the Joint Laboratory of Microsystems
† E-mail: yzhao@lnm.imech.ac.cn

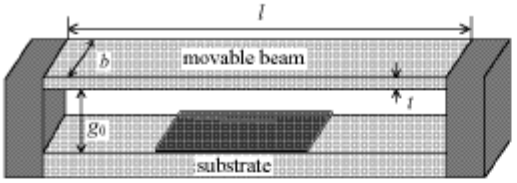

Fig.1 Schematic of a doubly supported RF MEMS switch

search duration. Presently the theory and model of the RF MEMS switches is mainly established on the conventional theories. The mostly referred formulation of critical pull-in voltage is

$$V_{\rm pi} = \sqrt{\frac{8K_{\rm eff}g_0^3}{27\varepsilon_0 A}} \tag{1}$$

which is derived from a 1D lumped model. However, by considering the miniaturization of structure and the coupling field effect, some new influential factors should be incorporated into the analysis of behavior of the RF MEMS switches, such as intrinsic residual stress from fabrication processes, axial stress due to stretching of beam, and fringing field effect. The relevant theory containing those factors was proposed[6], while numerical analysis of the RF MEMS switches was conducted by using FEM, BEM, or Shooting method[7,8].

In present paper we firstly by present a concise induction and analysis on our theoretical electromechanical model and the relevant influential factors. Subsequently based on the model, numerical calculation using a semi-analytical method is performed. The relationship between the characteristic of the RF MEMS switches and the relevant parameters is then further studied.

2 THE FORMULATIONS OF VARIOUS FACTORS

A simplified schematic drawing of the doubly supported switch is shown in Fig.2, where the transverse deflection w is uniform along the width of the movable beam, i.e., independent of the width. The middle point is defined as origin of the coordinate system. Because of the miniaturization, the couple field effect, and the special fabrication technology, the axial stretching of movable beam, the residual stress, and the fringing field effect have to be taken into account, respectively or simultaneously. Various influential factors[6] are presented concisely in this section.

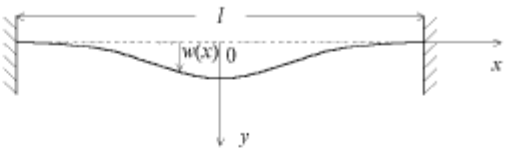

Fig.2 A schematic of the movable beam in a doubly supported switch

2.1 Axial Stress Due to Axial Stretching

The stretching is inevitable while a doubly clamped beam is bent. In some cases such as the maximum deflection less than the thickness of the beam, the stretching may be ignored. But for the RF MEMS switches, the original gap between two plates is often equal to or even larger than the thickness of the movable beam. Thereby the axial stress induced by the elongation of the movable beam has to be considered for more accurate models.

While a voltage is applied, the axial force T_a resulted from the elongation of the clamped beam is approximately given by

$$T_a = \frac{\tilde{E}bt}{2l}\int_{-l/2}^{l/2}\left(\frac{{\rm d}w}{{\rm d}x}\right)^2{\rm d}x \tag{2}$$

where $\tilde{E}$ is the equivalent modulus of the movable beam, and b, t and l are the width, thickness, and length of the movable beam, respectively. For a narrow beam $\tilde{E} = E$, where E is Young's modulus. For a wide beam $\tilde{E} = E/(1-\nu^2)$, where ν is Poisson's ratio[9].

2.2 Residual Stress Inherent in Microstructures

Residual stress is derived from the mismatch of both thermal expansion coefficient and crystal lattice period between the substrate and the upper beam during the fabrication processes[10,11].

Residual force may be formulated as

$$T_r = \hat{\sigma}bt \tag{3}$$

where $\hat{\sigma}$ is the residual stress, equal to $\sigma_0(1-\nu)$ for a doubly supported beam, where σ_0 is the biaxial residual stress.

2.3 Fringing Field Effect

A uniform magnetic or electric field cannot drop abruptly to zero at its edge, so a "fringing field" as shown in Fig.8 of Ref.[6] always exists in real situations. The fringing field is denoted by its first order correction, which is given as[10]

$$F_f = 0.65\frac{g_0 - w}{b} \tag{4}$$

3 NUMERICAL COMPUTATION OF THE MODEL

3.1 Formulation

Involving the various factors mentioned above, the equation governing the transverse deflection of the movable beam is written as

$$\tilde{E}\,\widehat{I}\,\frac{\partial^4 w}{\partial x^4}-(T_a+T_r)\frac{\partial^2 w}{\partial x^2}=\frac{\varepsilon_0 V^2 b}{2(g_0-w)^2}(1+F_f) \quad (5)$$

where V is the applied voltage, and ε_0 is the permittivity of air. The movable beam is assumed to have a rectangular cross section, thereby the moment of inertia of the cross section is $\widehat{I}=bt^3/12$. The problem is subject to boundary conditions as

$$w(0)=w(l)=0 \qquad \frac{\partial w}{\partial x}(0)=\frac{\partial w}{\partial x}(l)=0 \quad (6)$$

For convenience of analysis, dimensionless variables are introduced as

$$X=\frac{x}{l} \qquad W=\frac{w}{g_0} \qquad V'=\frac{V}{V_0} \quad (7)$$

where V_0 is the referenced voltage, which serves as a unit in the present computation and analysis.

Substituting Eq.(7) into Eq.(5), we obtain a new form of the governing equation as

$$\frac{\partial^4 W}{\partial X^4}-\Big[6\Theta_2\int_{-1/2}^{1/2}\Big(\frac{\mathrm{d}W}{\mathrm{d}X}\Big)^2\mathrm{d}X+12\Theta_3\Big]\frac{\partial^2 W}{\partial X^2}=$$

$$\Big[\frac{6\Theta_1}{(1-W)^2}V'^2+\frac{3.9\Theta_1 F_f}{(1-W)}V'^2\Big] \quad (8)$$

where

$$\Theta_1=\frac{\varepsilon_0 V_0^2 l^4}{\tilde{E}t^3 g_0^3} \quad (9a)$$

$$\Theta_2=\frac{g_0^2}{t^2} \quad (9b)$$

$$\Theta_3=\frac{\hat{\sigma}\,l^2}{\tilde{E}g_0^2} \quad (9c)$$

$$F_f=\frac{g_0}{b} \quad (9d)$$

which are dimensionless numbers equivalent to dimensionless number groups (Π_1,Π_2,Π_3,F_r)[6]. Θ_1 denotes the ratio of electrostatic force to bending force per unit length of the beam, Θ_2 is the ratio of the axial force due to elongation of the beam to bending force per unit length of the beam, Θ_3 is the ratio of the residual force inherent in the beam to bending force per unit length of the beam, and F_f is the first order fringing field correction number equal to the ratio of the initial gap between two plates to the width of the movable beam.

Considering the symmetry of microstructure and deformation along the X(i.e., x) direction, the boundary conditions can be equivalently rewritten as

$$W(0)=W(1/2)=0$$
$$\frac{\partial^3 W}{\partial^3 X}(0)=\frac{\partial W}{\partial X}\Big(\frac{1}{2}\Big)=0 \quad (10)$$

Equations (8) and (10) demonstrate that four dimensionless numbers Θ_1, Θ_2, Θ_3 and F_f denominate the transverse deflection of the movable beam under a given voltage. In the light of the expression given in Eq.(9b), when t is greatly larger than g_0, Θ_2 will become negligible, i.e., with sufficient accuracy the influence caused by the axial elongation of beam can be ignored. It is seen from Eq.(9c) that with the increasing of the length of the beam and the descending of the thickness of the beam, Θ_3 will play a more important role in the behavior of the microdevice.

3.2 Numerical Method Description

Equations (8) and (10) preclude the possibility of a closed-form solution, so we apply a polynomial approach to numerically solve the equations for $W(X)$. An initial deflection $W_0(X)=0$ is assumed under a certain voltage, and the next solution $W_1(X)$ is evaluated according to Eqs.(8) and (10). Then a convergent deflection $W(X)=W_n(X)$ may be gained by iterative computation. Since the microstructure and deformation along the X direction is symmetrical, polynomial $W_i(X)$ is assumed to be an even function

$$W_i(X)=a_0+a_1X^2+a_2X^4+\cdots+$$
$$a_{i-1}X^{2(i-1)}+a_iX^{2i} \quad (11)$$

For MEMS analysis, it was assumed that pull-in occurs when the microstructure deflects to 2/3 of the initial gap g_0[7]. Even though those influential factors can be expected to correct the obtained result, we assume that these corrections do not affect the above pull-in condition. Therefore the dimensionless form of deflection W should not be larger than 1/3 to avoid the occurrence of pull-in. Two terms in the right-hand side of Eq.(8) can be expanded as

$$f(W_i)=\frac{6\Theta_1}{(1-W_i)^2}V'^2=6\Theta_1V'^2\cdot$$
$$\big(1+2W_i+3W_i^2+\cdots+nW_i^{n-1}+\cdots\big) \quad (12a)$$

$$g(W_i) = \frac{3.9\Theta_1 F_f}{(1-W_i)} V'^2 = 3.9\Theta_1 F_f V'^2 \cdot \left(1 + W_i + W_i^2 + \cdots + W_i^{n-1} + \cdots\right) \quad (12b)$$

Here we take $n = 7$ to ensure a sufficient approximation.

For the second term of the left-hand side of Eq.(8), we denote

$$\phi(W_i) = 6\Theta_2 \int_{-1/2}^{1/2} \left(\frac{\mathrm{d}W_i}{\mathrm{d}X}\right)^2 \mathrm{d}X + 12\Theta_3 \quad (13)$$

According to Eqs.(12) and (13), in each iteration, we solve the nonlinear boundary-value problem

$$\frac{\partial^4 W_{i+1}}{\partial X^4} - \phi(W_i)\frac{\partial^2 W_{i+1}}{\partial X^2} = f(W_i) + g(W_i) \quad (14a)$$

$$W_{i+1}(0) = W_{i+1}\left(\frac{1}{2}\right) = 0$$

$$\frac{\partial^3 W_{i+1}}{\partial X^3}(0) = \frac{\partial W_{i+1}}{\partial X}\left(\frac{1}{2}\right) = 0 \qquad i = 0, 1, 2\cdots \quad (14b)$$

numerically for $W_{i+1}(X)$. The iteration ends when the error of the maximum of deflection curve falls into a tolerance (here given as 10^{-4}), or the maximum of dimensionless deflection is larger than 1/3. If $\left|(W_{i+1})_{\max} - (W_i)_{\max}\right| < 10^{-4}$, under the given applied voltage the microstructure reaches a stable state, i.e., the critical collapse voltage is not reached. And then an incremental voltage will be added, and the next iteration begins with an original deflection $W_0(X) = 0$. If $\left|W_{i+1}\right| > 1/3$, the upper movable beam will snap onto the lower substrate, and the critical pull-in voltage is reached.

To validate the obtained numerical results, we compare the results of the maximum deflection calculated using our approach to those reported by Choi and Lovell[12] in Fig.3 for a doubly clamped microbeam with $l = 400\,\mu$m, $b = 45\,\mu$m, $t = 2\,\mu$m, $g_0 = 1\,\mu$m, $\tilde{E} = 165$GPa and no axial load and no residual stress condition.

Otherwise we compare the critical pull-in voltage of the RF MEMS switches obtained using our approach with some existed models and experimental results[13], as shown in Fig.4. Using the dimensionless numbers introduced above, the existed models can be rewritten as

$$\frac{V_{\mathrm{pi}}}{V} = \frac{2\pi^2}{5}\sqrt[4]{\frac{3}{5}}\sqrt{\frac{1}{\Theta_1}} \quad (15)$$

$$\frac{V_{\mathrm{pi}}}{V} = \frac{16}{3\sqrt{3}}\sqrt{\frac{1}{\Theta_1}} \quad (16)$$

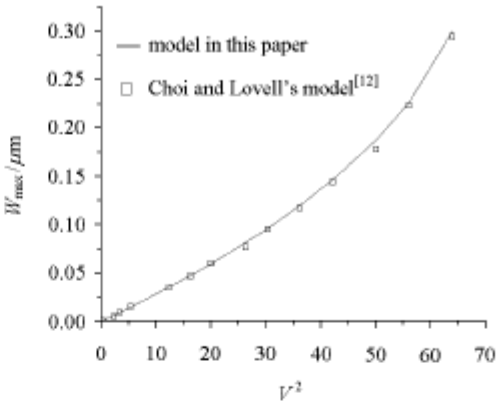

Fig.3 Comparison of the maximum defection $W_{\max}$ for $\Theta_2 = 0$, and $\Theta_3 = 0$

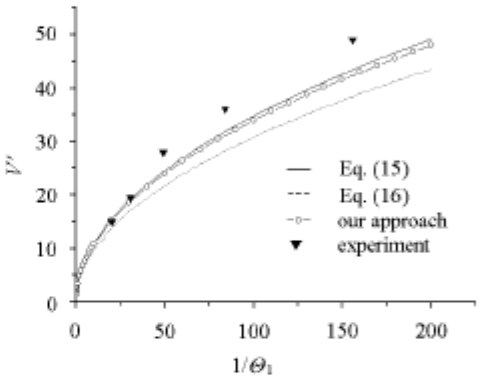

Fig.4 Comparison of the dimensionless critical pull-in voltage V' of the RF MEMS switches

Here Eq.(15) is approximately resulted from Rayleigh-Ritz energy method[13]; and Eq.(16) is derived from a 1D lumped model[7]. Due to the assumptions made for the 1D lumped model, the real voltage is expected to be smaller than the actual value shown in Fig.4. The difference between prediction of these theoretical models and the experimental results will be larger with increasing $1/\Theta_1$. Since the residual stress and the axial stretching of the beam can increase the critical threshold voltage, taking those influential factors into account will help to obtain more accurate theoretical results. In the following section 4 we will research into the influence of various relevant parameters on the model introduced in the present paper.

4 RESULTS DISCUSSION AND ANALYSIS

The behavior of the RF MEMS switches governed by Eq.(5) is dependent on many physical parameters. On the other hand, as combinations of

those physical parameters, four dimensionless numbers which we introduced in Eq.(9) can be regarded as dominated parameter groups. Here we analyze the influences of those physical parameters and dimensionless numbers respectively and compare the relative importance of those parameters in order to improve the design and fabrication of the micro devices.

4.1 Discussion on Physical Parameters

The mechanical properties and material parameters of the microstructures used in the present calculation are listed in Table 1.

Table 1 Material and geometrical parameters

Parameters	Value
Young's modulus, E/GPa	76.52
Poisson's ratio, ν	0.41
permittivity of air, $\varepsilon_0/(\mathrm{F\cdot m^{-1}})$	8.854×10^{-12}
length of the beam, l/μm)	100~1 000
width of the beam, b/μm	60~150
thickness of the beam, t/μm	1.0~1.8
initial gap, g_0/μm	0.8~3.0

In view of the governing equation shown as Eq.(5), it is expected that the critical pull-in voltage of the switch structures depends on their geometric and material properties, such as the length l, the width b, the thickness t, the initial gap g_0, Young's modulus E, Poisson's ratio ν, and residual stress σ. Since the materials used in the RF MEMS switches fabrication at present are relatively fixed, here we mainly discuss the influences of geometric parameters and residual stress.

The dependence of the critical pull-in voltage on the length of movable beam and residual stress is shown in Fig.5, where the initial gap $g_0 = 1.5\,\mu$m, the thickness $t = 1.5\,\mu$m, and the width $b = 90\,\mu$m. This figure shows that the residual stress contributes remarkably to the critical voltage of the microstructure. The larger residual stress is, the larger the critical pull-in voltage is. On the other hand, the threshold voltage decreases with the increase of the length of the movable beam; and when the length is large enough, the threshold voltage is almost prone to one steady value, i.e. the influence of the length becomes inconspicuous.

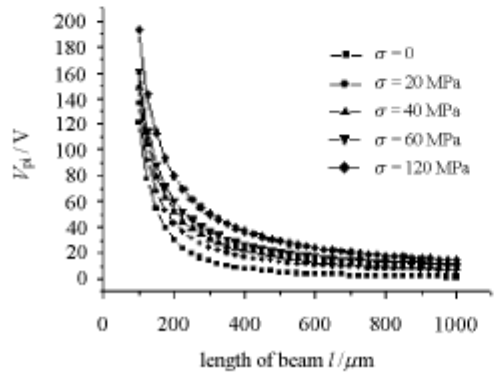

Fig.5 The critical pull-in voltage V_{pi} as function of the length of the beam with various residual stresses

The relationship between the pull-in critical voltage and the initial gap of movable beam is shown in Fig.6, whilst $g_0 = 1.5\,\mu$m, $b = 90\,\mu$m, and $\sigma = 0$ are taken in the computation. The figure illustrates that the critical threshold voltage is sensitive to the initial gap of the structure. This sensitivity is dependent on the length of the beam, for example, when the initial gap increases from $0.8\,\mu$m to $3.0\,\mu$m, the pull-in voltage varies from 11.5 V to 93.6 V for $l = 200\,\mu$m, but from 1.3 V to 10.4 V for $l = 600\,\mu$m.

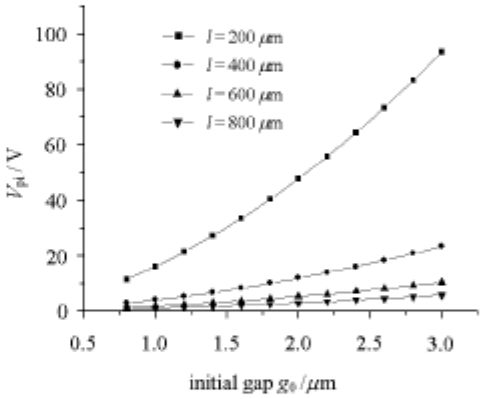

Fig.6 The critical pull-in voltage V_{pi} as function of initial gap with various lengths of the beam

When residual stress $\sigma = 0$, the influence of the thickness of the movable beam on the critical pull-in voltage is depicted in Fig.7, where $g_0 = 1.5\,\mu$m, $b =$

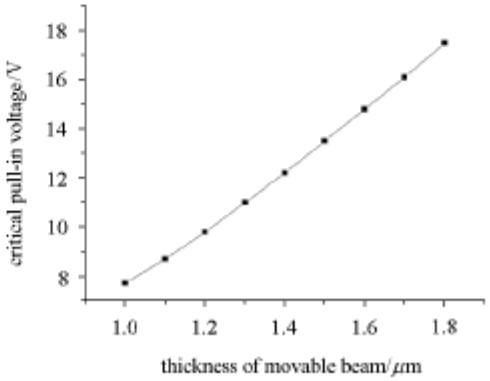

Fig.7 The critical pull-in voltage as function of the thickness of the beam with $g_0 = 1.5\,\mu$m, $b = 90\,\mu$m, $l = 300\,\mu$m, and $\sigma = 0$

$90\,\mu$m, and $l = 300\,\mu$m are taken in the computation. The figure shows that the threshold voltage is sensitive to the thickness of the movable beam.

In view of Eq.(9d), the influence of the width of movable beam b is similar with that of $1/F_f$ when the initial gap g_0 is specified. From the calculated results and the relevant analysis of $1/F_f$ shown in the following section, it will be seen that the influence of the width b is trivial.

Considering the influences of various geometry parameters and residual stress shown above, those influential parameters should be all taken into account in the mechanical design and optimization of the RF MEMS switches. An alternative approach, which replaces the analysis for those physical parameters, introducs dimensionless numbers into analysis of characteristics, as given below.

4.2 Discussion on Dimensionless Parameter Groups

As shown in Eq.(9), dimensionless group Θ_1 presents the competition between the bending force and electrostatic force per unit length of the beam, and Θ_2, Θ_3, F_f are relevant to the axial stress, residual stress, and fringing field effect, respectively.

The relationships between dimensionless critical pull-in voltage V' and Θ_1 for various values of Θ_2 and Θ_3 are shown in Fig.8 and Fig.9, respectively. The both figures illustrate that the critical pull-in voltage increases with increasing of Θ_2 or Θ_3, i.e., the larger the effect of axial stretching and the residual stress are, the higher the critical pull-in voltage is. The comparison of the influences of Θ_2 and Θ_3 on the critical pull-in voltage is given in Fig.10, which indicates that Θ_3 is more sensitive than Θ_2.

The influence of F_f on the dimensionless critical pull-in voltage is shown in Fig.11. By considering

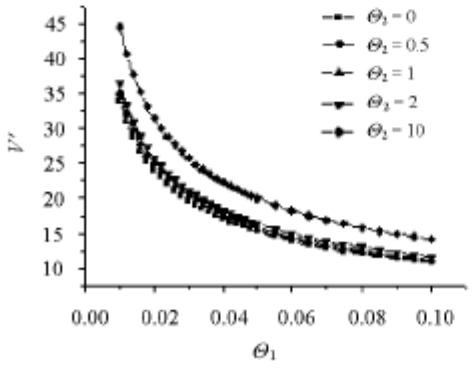

Fig.8 The dimensionless form of critical pull-in voltage V' as function of Θ_1 with various Θ_2, whilst $\Theta_3 = 0$ and $F_f = 0$

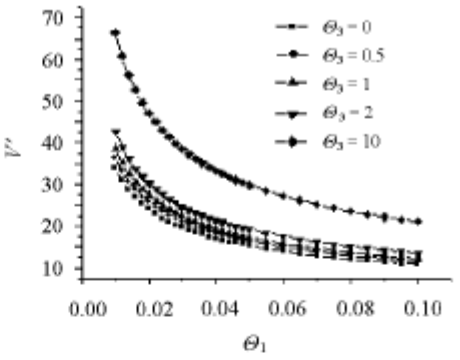

Fig.9 The dimensionless form of critical pull-in voltage V' as function of Θ_1 with various Θ_3, whilst $\Theta_2 = 0$ and $F_f = 0$

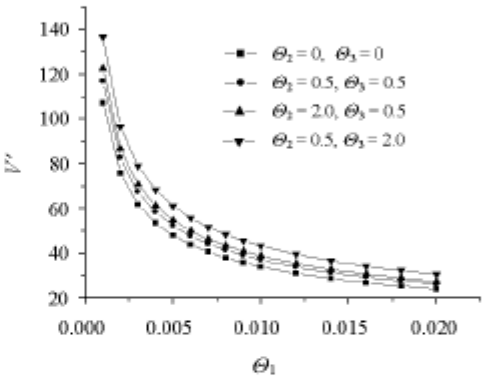

Fig.10 The dimensionless form of critical pull-in voltage V' as function of Θ_1 with various Θ_2 and Θ_3, whilst $F_f = 0$

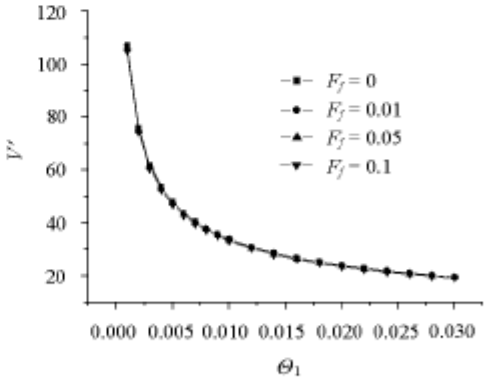

Fig.11 The dimensionless form of critical pull-in voltage V' as function of Θ_1 with various F_f, whilst $\Theta_2 = 0$ and $\Theta_3 = 0$

the typical values of initial gap g_0 and width b given in Table 1, F_f should be around 0.01. The figure illustrates that the variation of the critical pull-in voltage resulted from the variation of F_f is trivial in an extensive range. Since the width b is much larger than

the initial gap g_0, it is concluded that the influence of the width of the beam is trifling to the threshold voltage.

From Figs.8∼11 it is seen that among the considered influential factors, the influences of axial stretching and residual stress are remarkable and should be taken into account in the design and optimization of the RF MEMS switches. Furthermore, the residual stress is more sensitive than the axial stretching of beam. The fringing field effect is negligible in comparison with the above two factors within a certain range.

5 CONCLUSIONS

In the present paper we studied a newly-developed model of the RF MEMS switches, which takes into account of the axial stretching of beam, the residual stress inherent in the structure, and the fringing field by using a polynomial approximate approach. The calculated results from our approach are validated (see Fig.3). Compared with some existed models and experimental results, the developed model is able to give a more accurate theoretical prediction of the critical threshold voltage for the doubly clamped switch structure.

The sensitivity of the critical pull-in voltage on the geometry parameters and the residual stress is analyzed. Figures 5∼7 demonstrate that the change of the length, the initial gap, the thickness, and the residual stress can remarkably affect the critical pull-in voltage. Whilst in some special cases such as when the length of the movable beam is adequately large, the sensitivity of the threshold voltage on those independent variables would be reduced. On the other hand, four dimensionless numbers are derived from the governing equation, and their influences on the critical pull-in voltage are analyzed. Calculated results show that Θ_2 and Θ_3, representing the influences of the residual stress and the axial stretching of the beam, respectively, play significant roles (see Fig.8 and Fig.9), but F_f, representing the fringing field effect, is secondary compared with the former two (see Fig.11). The accurate prediction of the behavior of the microstructure based on our new approach will facilitate designers to select various parameters and influential factors within a wide range in their designs.

REFERENCES

1 Yao JJ. Topical review: RF MEMS from a device perspective. *J Micromech Microeng*, 2000, 10: R9∼R38

2 Nguyen CT. Microelectromechanical devices for wireless communications. In: IEEE MEMS'98, Heidelberg, Germany, 1998. 1∼7

3 Feng ZP, Zhang HT, Zhang WG, et al. MEMS-based variable capacitor for millimeter-wave applications. In: Proceedings of Solid-State Sensor and Actuator Workshop, Hilton Head Island, South Carolina, 2000. 255∼258

4 Elders J, Spiering V, Walsh S. Microsystems Technology (MST) and MEMS applications: an overview. *Microelectromechanical Systems: Technology and Applications* (MRS Bulletin), 2001, 26 (4): 312∼317

5 Peterson KE. Micromechanical membrane switches on silicon. *IBM J Res Dev*, 1979, 23: 376∼385

6 Zhang LX, Zhao YP. Electromechanical model of RF MEMS switches. Microsystem Technologies, 2003, 9(6-7): 420∼426

7 Osterberg PM. Electrostatically actuated micromechanical test structures for material property measurement. [Ph D Dissertation], MIT, Cambridge, MA, 1995

8 Huang JM, Liew KM, Wong CH, et al. Mechanical design and optimization of capacitive micromachined switch. *Sensors and Actuators*, 2001, A(93): 273∼285

9 Temoshenko S. Theory of plates and shells. McGraw-Hill, Inc, 1987

10 Qian J, Liu C, Zhang DC, et al. Residual stress in micro-electro-mechanical systems. *Journal of Mechanical Strength, Special Issue on MEMS*, 2001, 23(4): 393∼401 (in Chinese)

11 Pauleau Y. Generation and evolution of residual stress in physical vapour-deposited thin films. *Vacuum*, 2001, 61: 175∼181

12 Choi B, Lovell EG. Improved analysis of microbeams under mechanical and electrostatic loads. *J Micromech Microeng*, 1997, 7: 24∼29

13 Gupta RK. Electrostatic pull-in test structure design for in-situ mechanical property measurements of Micro-Electro-Mechanical Systems (MEMS). [Ph D Dissertation], the Massachusetts Institute of Technology, USA, 1997